Journal of Alloys and Compounds 714 (2017) 419–424

Contents lists available at ScienceDirect

Journal of Alloys and Compounds

journal homepage: http://www.elsevier.com/locate/jalcom

Hedgehog-like CuO/nitrogen-doped graphene nanocomposite for high-performance lithium-ion battery anodes

Ji-Xiang Chen, Dong-Lin Zhao*, Ran-Ran Yao, Cheng Li, Xia-Jun Wang, Fei-Fei Sun

State Key Laboratory of Chemical Resource Engineering, Key Laboratory of Carbon Fiber and Functional Polymers, Ministry of Education, Beijing Engineering Research Center of Environmental Material for Water Purification, Beijing University of Chemical Technology, Beijing 100029, China

ARTICLE INFO

Article history:
Received 3 January 2017
Received in revised form
1 April 2017
Accepted 14 April 2017
Available online 17 April 2017

Keywords:
Energy storage materials
Electrode materials
Nanostructured materials
Oxide materials
Nanofabrications

ABSTRACT

With a hydrothermal method, we have successfully prepared hedgehog-like CuO/nitrogen-doped graphene nanosheet (CuO/N-GNS) nanocomposite. The hedgehog-like CuO/N-GNS nanocomposite exhibits superior Li-ion storage properties in terms of high capacity, long cycle life, and excellent rate performance. After 50 cycles, hedgehog-like CuO/N-GNS nanocomposite exhibits higher discharge special capacity (750.1 mA h g^{-1}) than hedgehog-like CuO (456.8 mA h g^{-1}) at a current of 100 mA g^{-1}. The cyclic stability of hedgehog-like CuO/N-GNS nanocomposite is better than that of hedgehog-like CuO, indicating that N-GNSs can further improve the cycle performance of hedgehog-like CuO owing to its high electrical conductivity and good buffer role. The hedgehog-like CuO/N-GNS nanocomposite has potential applications in the anodes of lithium-ion batteries.

1. Introduction

For now, high-performance lithium-ion batteries (LIBs) have found widespread applications in portable electronic devices such as mobile phones as well as in various kinds of electric vehicles. With LIBs existing some problems that applications in electronic equipment and electric vehicles, so it is necessary to develop high-performance anode materials which have long cycle life, high capacity and good rate capability [1–3].

CuO is a competitive candidate in anode materials of LIBs that can be attributed to low cost, chemical stability, environmental friendly nature, high safety and high theoretical capacity (674 mA h g^{-1}). However, electrode pulverization and the loss of electrical contact during repetitive cycling lead to non-ideal cycle life and poor rate performance so that limits the application of CuO [4,5]. In order to deal with these problems, researchers usually alleviate the adverse mechanical effects to improve the overall electrochemical performance of CuO anodes by coupling with a conductive matrix or construction of various nanostructures.

In this paper, we have successfully prepared hedgehog-like CuO/nitrogen-doped graphene nanosheet (CuO/N-GNS) nanocomposite by a hydrothermal method. At the same time, we conclude that hedgehog-like CuO/N-GNS nanocomposite has higher capacity at the same current rate, better cycling performance and rather excellent rate performance than those of hedgehog-like CuO. The present result shows that it is potential to apply hedgehog-like CuO/N-GNS nanocomposite to portable electronic devices or electric vehicles.

2. Experimental

2.1. Synthesis of N-GNSs

Graphene oxide (GO) nanosheets were prepared in two steps: the oxidation of flake natural graphite powder via a modified Hummers' method and ultrasonication. $KMnO_4$ was employed as the oxidant to obtain graphite oxide [6,7]. Firstly, 1 g of flake natural graphite powder with the mean diameter of 15 μm (provided by Dong Xing Electrical Carbon Co., Ltd. China) was added to 23 mL of cooled (0 °C) concentrated H_2SO_4. Then 3 g of $KMnO_4$ was added gradually with stirring and cooling, so that the temperature of the mixture was maintained below 10 °C. The mixture was then stirred at 35 °C for 30 min. After this, 46 mL of distilled water was slowly added to cause an increase in temperature to 98 °C and the mixture was maintained at that temperature for 15 min. The reaction was terminated by adding 140 mL of distilled water followed by 10 mL

* Corresponding author.
E-mail address: dlzhao@mail.buct.edu.cn (D.-L. Zhao).

http://dx.doi.org/10.1016/j.jallcom.2017.04.171
0925-8388/

of 30% H_2O_2 solution. The suspension was then repeatedly centrifuged and washed twice with 5% HCl solution and then repeatedly with water until sulfate could not be tested with barium chloride. The collected precipitate was dispersed in 450 mL water and sonicated for 2 h. Then the suspension was separated into the supernatant liquor and a golden colored residue by centrifugation at 5000 rpm for 10 min. The supernatant was centrifuged again at 15000 rpm for 5 min to remove the suspended substance. The precipitate was ultrasonicated, collected and dried in a vacuum oven at 60 °C, thus GO nanosheets were obtained.

The N-GNSs were synthesized through a one-pot hydrothermal process using urea as the chemical dopant in the presence of GO aqueous dispersion. Typically, 80 mg GO nanosheets were dispersed into deionized water (80 mL) through agitation and was stirred at 30 °C for 1 h to obtain the GO nanosheet dispersion. And then 10 g urea was added into the GO nanosheet dispersion under sonication for 3 h. After that, the solution was sealed in a 100 mL Teflon-lined autoclave and maintained at 180 °C for 12 h. The solids (N-GNSs) were filtered and washed with distilled water several times. Finally, the collected N-GNSs were dried in a vacuum oven at 80 °C for 10 h.

2.2. Synthesis of hedgehog-like CuO/N-GNS nanocomposite

In a typical synthesis, 1.06 g $Cu(NO_3)_2 \cdot 3H_2O$ and 40 mg N-GNSs were first dissolved in 50 mL of absolute alcohol to form a solution, and then 30 mL of ammonia water (25%), 10 mL of 1 mol/L sodium hydroxide and 2.0 g of sodium nitrate were added respectively. After stirring for 10 min to form a clear solution, the resulting solution was sealed in a 100 mL Teflon-lined autoclave and maintained at 130 °C for 18 h. The resulting precipitate solid was collected by centrifugation, washed with distilled water and absolute ethanol. Finally, the collected CuO/N-GNS nanocomposites were drying in a vacuum oven at 60 °C for 8 h. The hedgehog-like CuO without N-GNSs was also prepared using the same process for comparison purposes.

2.3. Characterization of materials

The morphology and structure of the samples were observed by scanning electron microscope (SEM, Hitachi S-4700) and high-resolution transmission electron microscope (HRTEM, JEOL 3010). X-ray diffraction (XRD) analysis was conducted on a Rigaku D/max-2500B2+/PCX system using Cu/Kα radiation (λ = 1.5406 Å). The information of functional groups was measured by Fourier transform infrared spectroscopy instrument (FTIR, Nicolet Nexus 670). X-ray photoelectron spectroscopy (XPS) analysis was performed on a Thermo Fisher ESCALAB250xi with an MgKa (1253.6 eV) achromatic X-ray source.

2.4. Electrochemical measurements

The electrochemical performances of hedgehog-like CuO and hedgehog-like CuO/N-GNS nanocomposites were measured with the coin-type cells. The lithium sheets were used as both reference and counter electrodes, and composite electrodes comprising active mass (hedgehog-like CuO or hedgehog-like CuO/N-GNS nanocomposites, 85 wt.%), carbonaceous additive (acetylene black, 5 wt.%) and poly(vinylidene difluoride) (PVDF, 10 wt.%) binder were used as working electrodes. 1 M $LiPF_6$ solution in a 1:1 (volume) mixture of ethylene carbonate (EC) and dimethyl carbonate (DMC) from Merck Co. was used as electrolyte. The Celgard 2400 microporous polypropylene film provided by Jimitek Electronic (Shenzhen) Co. Ltd was used as separator. The coin-type cells were galvanostatically discharged (Li insertion) and charged (Li extraction) in the voltage range from 0.01 to 3.0 V vs. Li/Li^+ at the different current densities. Electrochemical impedance spectroscopy measurements of the electrodes were carried out on an electrochemical workstation (Princeton VersaSTAT3-200) using the frequency response analysis. Cyclic voltammogram (CV) was obtained in the voltage of 0–3 V at a scanning rate of 0.1 mV/s at room temperature. The impedance spectra were obtained by applying a sine wave with amplitude of 5.0 mV over the frequency range from 100 kHz to 0.01 Hz.

3. Results and discussion

Fig. 1 shows the XRD patterns of hedgehog-like CuO, N-GNSs and hedgehog-like CuO/N-GNS nanocomposite. The CuO/N-GNS nanocomposite displays broader peaks than the bare CuO, but shows lower intensity, suggesting that the CuO/N-GNS composite is composed of small CuO particles with relatively low crystallization, owing to the high density of oxy-gen functional groups, including carboxylic, hydroxyl, and epoxy groups, on GO surface to hinder diffusion, crystallization and growth of CuO grains [8–10]. All peaks can be indexed as monoclinic CuO phase by comparison with the JCPDS card files no.48-1548. No other impurity peaks are detected, indicating that the product is rather pure.

Fig. 2 shows the SEM images of hedgehog-like CuO (a), hedgehog-like CuO/N-GNS nanocomposite (b), N-GNS (c), and TEM images of N-GNSs (d), hedgehog-like CuO (e), hedgehog-like CuO/N-GNS nanocomposite (f). Fig. 2c and d exhibit the SEM and TEM images of N-GNSs, showing that the N-GNSs are ultrathin sheets with wavy structures. Fig. 2c exhibits the SEM image of N-GNSs agglomerate, consisting of almost transparent carbon nanosheets with thin wrinkled structure. N-GNSs are entangled with each other and resemble crumpled papers as shown in Fig. 2d. Moreover, the thin wrinkled structure represents a curled and corrugated structure that the graphene owns intrinsically.

Fig. 2a, b, e, and f show the typical SEM and TEM images of hedgehog-like CuO and hedgehog-like CuO/N-GNS nanocomposite. Fig. 2a reveals that the hedgehog-like CuO microspheres are very uniform with a size of 3–5 μm. Several conjoint spheres can be clearly seen, and the surfaces of these spheres are rough. Fig. 2e shows a representative TEM image of the hedgehog-like CuO, from which these sphere-like hedgehog are composed of many nanorods. When the N-GNSs were added, Fig. 2b and d shows that the

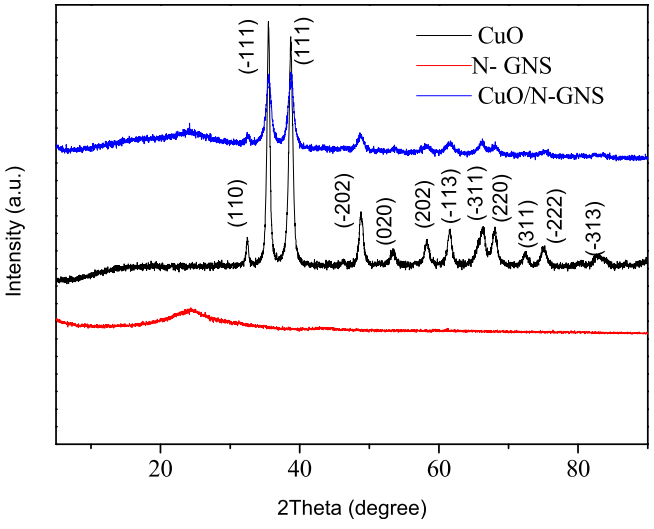

Fig. 1. XRD patterns of the hedgehog-like CuO, N-GNSs and hedgehog-like CuO/N-GNS nanocomposite.

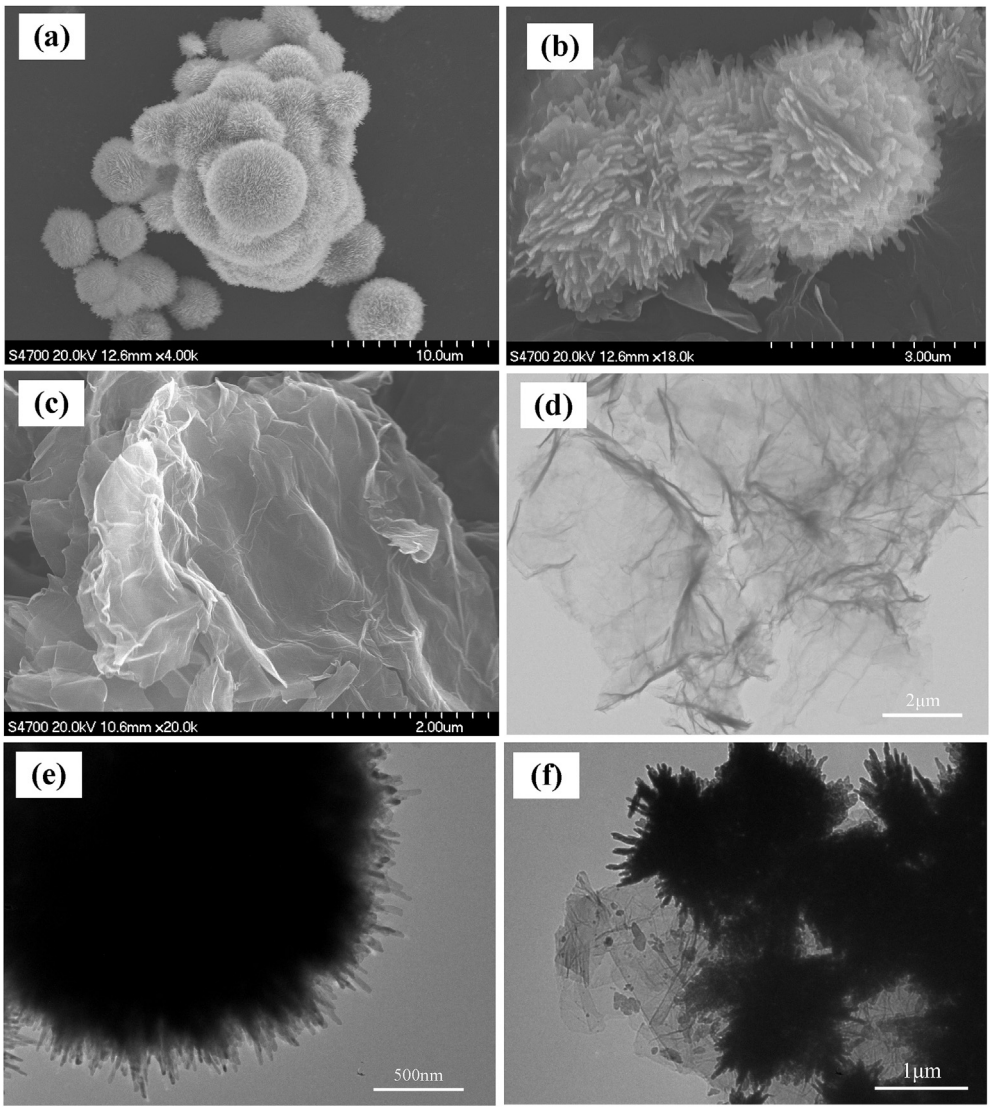

Fig. 2. SEM images of hedgehog-like CuO (a), hedgehog-like CuO/N-GNS nanocomposite (b), N-GNSs (c), TEM images of N-GNSs (d), hedgehog-like CuO (e), hedgehog-like CuO/N-GNS nanocomposite (f).

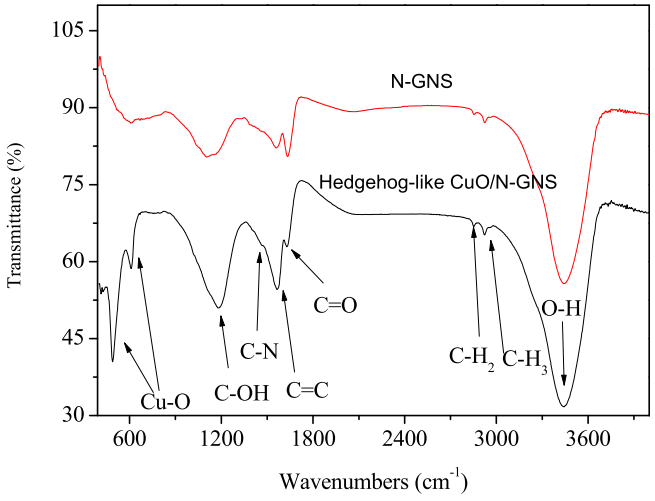

Fig. 3. FTIR spectra of hedgehog-like CuO/N-GNS nanocomposite and N-GNSs.

flower-like CuO and N-GNSs are uniformly dispersed.

Fig. 3 shows FTIR spectra of the hedgehog-like CuO and hedgehog-like CuO/N-GNS nanocomposite. The band appears at 550 cm^{-1} which is the characteristic absorption band arising from the stretching and bending modes of Cu–O bond [11]. A broad peak centeres at 3306 cm^{-1} that is because of the OH stretching of physical absorbed water on the composite surface [12]. The FTIR spectra strongly indicate the presence of abundant hydroxyl groups on composite surface, which plays an important role in the composite stability. The band at 1650 cm^{-1} is assigned to the C=O stretching mode of quinone groups while the band at 1581 cm^{-1} is assigned to C=C double bonds located near the newly formed oxygenated groups [13]. The peaks between 1430 cm^{-1} and 1480 cm^{-1} are related to the sp^3 C–N [14,15]. So it turns out that hedgehog-like CuO anchors on the N-GNSs. A broad band centered at 1153 cm^{-1} is associated with C=O stretching vibrations [16].

To investigate the N-doping effect in graphene, XPS was carried out to evaluate the chemical composition of N-GNS sample. The typical XPS spectra of N-GNSs are displayed in Fig. 4. Fig. 4a shows a C1s XPS spectrum of N-GNSs. Five types of carbon which correspond to carbon atoms in different functional groups appear clearly.

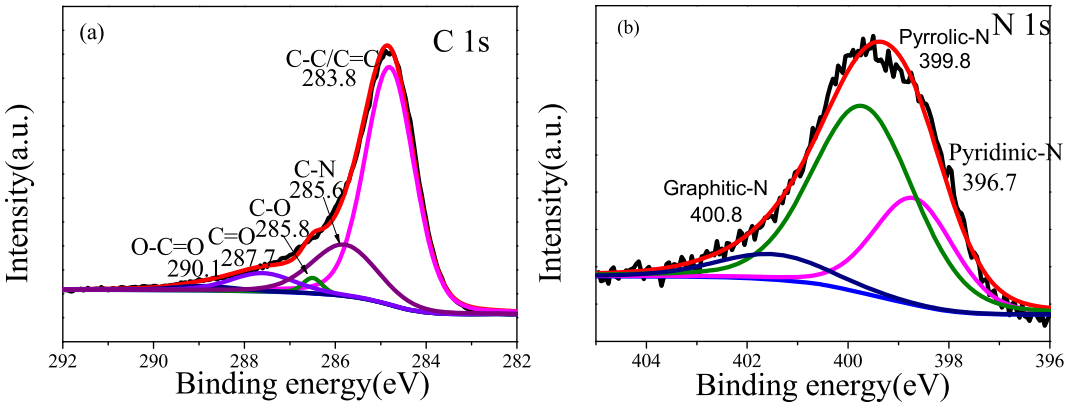

Fig. 4. The C1s XPS spectrum (a) and N1s XPS spectrum (a) of N-GNSs.

The C 1s peak of C—C/C=C is observed at 283.8 eV, C1s of C—N at 285.6 eV, C1s of C—O at 285.8 eV, C1s of C=O at 287.7 eV, and C1s of O—C=O at 290.1 eV, respectively. The N1s XPS spectrum of N-GNSs is displayed in Fig. 4b. Generally, the peaks locates at 396.7, 399.8, 400.8 eV are assigned to the pyridinic-, pyrrolic-, and graphitic-type of N atoms doped in the graphene structure. The N content in the N-GNSs is determined to be 9.24 at%. It confirms that N was successfully doped in the GNSs.

Fig. 5 displays the CV measurement of hedgehog-like CuO/N-GNS nanocomposite and hedgehog-like CuO in the potential range of 0.01–3.0 V at a scanning rate of 0.2 mV s^{-1}. In the first cycle, there are three cathodic peaks. As shown in Fig. 5, for the first cathodic scan of hedgehog-like CuO/N-GNS nanocomposite, there is a weaker broad peak at 2.20 V, which is combined with the solid solution formation (Li_xCuO). The sharp peak around 1.0 V is associated with the formation of Cu_2O phase [17]. In addition, most of irreversible electrolyte decomposition also takes place in the latter potential cannot be ruled out [18]. In the anodic scan, broader oxidation potential 2.53 V is attributed to the formation of Cu_2O ($2Cu + Li_2O \rightarrow Cu_2O + 2Li$) and the oxidation of Cu_2O into CuO as well [19,20]. For the hedgehog-like CuO and hedgehog-like CuO/N-GNS nanocomposite electrode, in the subsequent scanning cycles, the intensities of the cathodic peaks are decreasing due to the irreversible reaction ($CuO + 2Li \rightarrow Cu + Li_2O$) and the formation of the solid electrolyte interface (SEI) film [21]. After the 1st cycle, the curves of the second and the 3rd cycle are similar in shape, indicating that the electrode reactions become more reversible [22]. However, it easily can be found that the reduction peak and oxidation of hedgehog-like CuO/N-GNS nanocomposite are all shifted to the left and more coincident, suggesting more reversible during cycling than hedgehog-like CuO.

In order to demonstrate the electrochemical performance of hedgehog-like CuO after adding N-GNSs, we carried out electrochemical investigation. Fig. 6 shows the charge/discharge curves of hedgehog-like CuO and hedgehog-like CuO/N-GNS nanocomposite for the 1st and 2nd cycles at a current of 100 mA g^{-1} in the voltage range of 0.01–3 V. The first discharge and charge capacities of the hedgehog-like CuO and hedgehog-like CuO/N-GNS nanocomposite are 1506.3 and 859.6 mAh g^{-1}, 1073.3 and 601.3 $mAhg^{-1}$, respectively. Therefore, the first discharge/charge special capacities of hedgehog-like CuO/N-GNS nanocomposite are higher those of hedgehog-like CuO, which may be attributed to the conductive network between hedgehog-like CuO and N-GNSs. In the first discharge curve, the plateau at about 1.0 V was attributed to the reduction of CuO to Cu [23]. In the following cycling process, the discharge plateau shifted to about 0.9 V. In the discharge-charge curves of hedgehog-like CuO/N-GNS nanocomposite, we can see that the discharge-charge voltage profiles of hedgehog-like CuO is similar to that of CuO/N-GNS nanocomposite. Otherwise, the inclined plateaus about 1.4 V and 2.3 V can be showed in the first

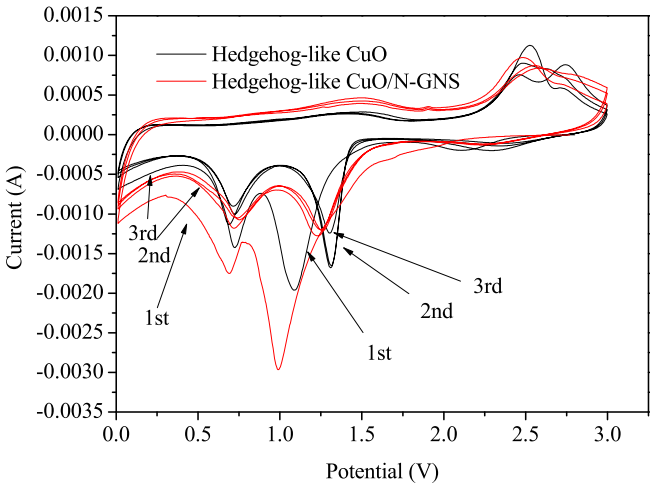

Fig. 5. The CV of hedgehog-like CuO/N-GNS nanocomposite and hedgehog-like CuO.

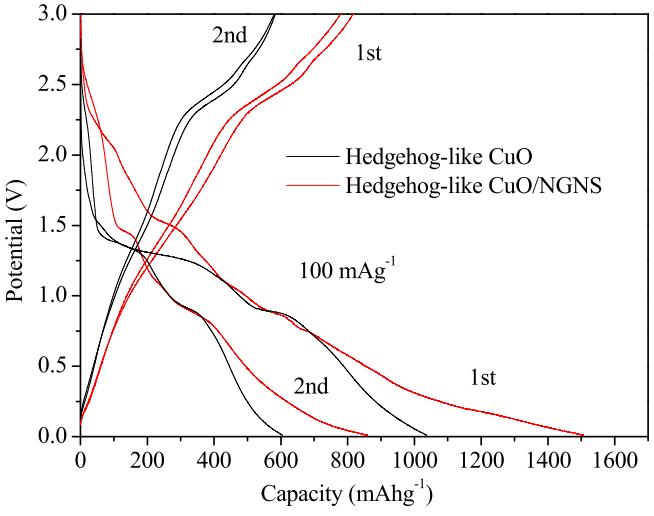

Fig. 6. Discharge-charge curves of hedgehog-like CuO/N-GNS nanocomposite and hedgehog-like CuO.

charge curves, corresponding to the process of $2Cu + Li_2O \rightarrow Cu_2O + 2Li + 2e^-$ and the partial oxidation of Cu_2O to CuO, respectively. The coulombic efficiency of CuO/N-GNS nanocomposite in the first cycle is about 66%, but it increase to about 96% in the second cycle.

In Fig. 7, the hedgehog-like CuO/N-GNS electrode shows better cycle performance than hedgehog-like CuO at a current density of 100 mA g^{-1}. The hedgehog-like CuO/N-GNS nanocomposite displays 713.1 mA h g^{-1} after 50 cycles, while hedgehog-like CuO only keeps 383.5 mA h g^{-1}. The cyclic stability of hedgehog-like CuO/N-GNS nanocomposite is better than that of hedgehog-like CuO, indicating that N-GNSs can further improve the cycle performance of CuO owing to its high electrical conductivity and good buffer role.

The rate capability is another important parameter required in the LIB application. Fig. 8 shows the rate performance of as prepared hedgehog-like CuO/N-GNS nanocomposite and hedgehog-like CuO electrode. The discharge/charge capacities of hedgehog-like CuO/N-GNS nanocomposite are higher than those of hedgehog-like CuO at the same current rate. The main reason is as the following benefits: (I) N-GNSs can promote the conductivity of hedgehog-like CuO, enlarge the lithium ions to contact with the electrode and shorten lithium ions route of transmission. (II) N-GNSs can buffer the change of volume to keep the structure stability during discharging and charging. The average capacity of hedgehog-like CuO/N-GNS nanocomposite at a galvanostatic current density of 50 mA g^{-1}, 100 mA g^{-1}, 200 mA g^{-1}, 500 mA g^{-1} and 1000 mA $g^{-1}$is 605, 593, 589, 570 and 485 mA h g^{-1}, respectively, but the average capacity of hedgehog-like CuO is 585, 405, 375, 189 and 98 mA h g^{-1}, respectively. With increasing the current rate from 50 to 1000 mA g^{-1}, the capacity of hedgehog-like CuO/N-GNS nanocomposite decreases by only 3.3%, while hedgehog-like CuO (83.2%). Otherwise, at 50 mA g^{-1} current rate, the capacity of hedgehog-like CuO/N-GNS nanocomposite recovers 695 mA h g^{-1}, but hedgehog-like CuO can only regain 580 mA h g^{-1}.

In order to further compare the electrochemical properties of hedgehog-like CuO/N-GNS nanocomposite and hedgehog-like CuO electrodes, their Nyquist complex plane impedance plots are presented in Fig. 9a. The equivalent circuit model of the studied system is shown in Fig. 9b. R_s presents the resistance of the electrolyte. R_{SEI} and CPE1 are related to the resistance and constant phase element of SEI film, R_{ct} and CPE2 are associated with the charge-transfer resistance and constant phase element of the electrode/electrolyte interface, and Z_W represents the Warburg impedance related to lithium ion diffusion [24–27]. In Fig. 9a, the diameter of hedgehog-like CuO/N-GNS nanocomposite is smaller than that of hedgehog-like CuO in the high frequency region, implying hedgehog-like CuO/N-GNS nanocomposite has a lower charge transfer resistance. Therefore, N-GNSs can improve the conductivity of hedgehog-like CuO.

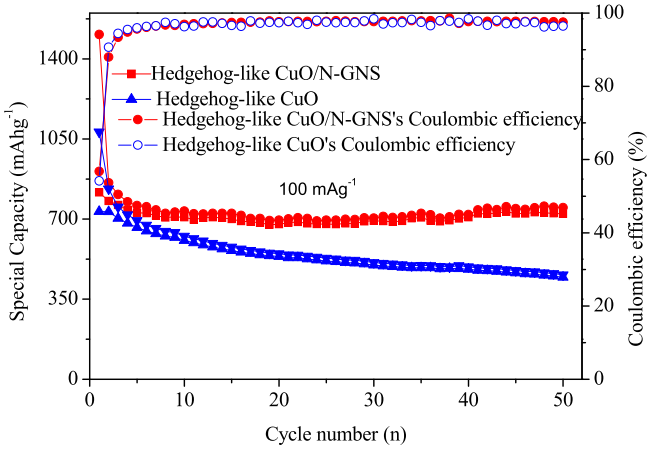

Fig. 7. Cycling performance of hedgehog-like CuO/N-GNS nanocomposite and hedgehog-like CuO at a current rate of 100 mA g^{-1}.

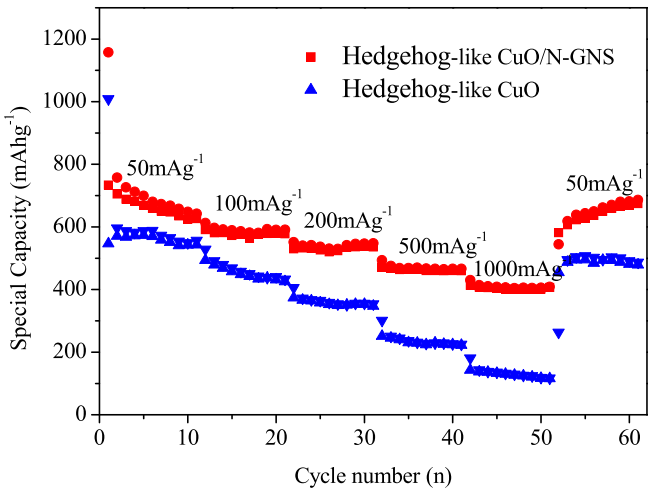

Fig. 8. Cycling performance of hedgehog-like CuO/N-GNS nanocomposite and hedgehog-like CuO at different rates.

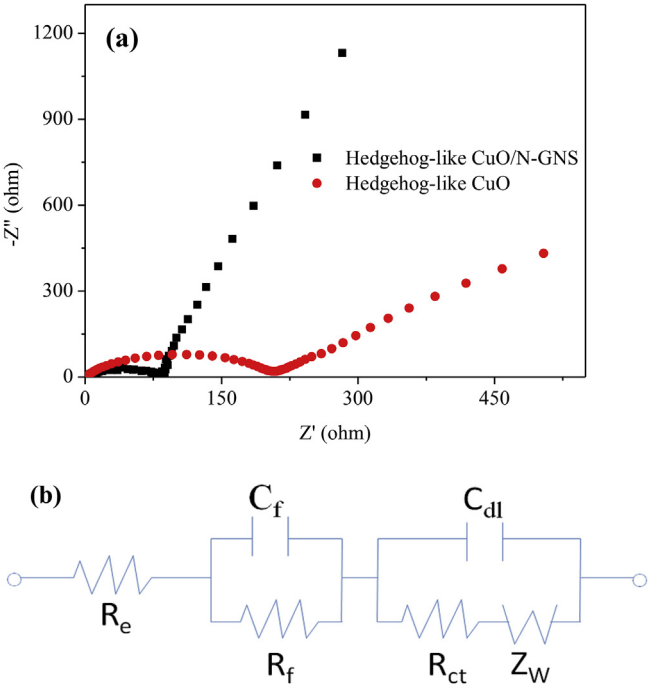

Fig. 9. Nyquist plots of impedance for hedgehog-like CuO and hedgehog-like CuO/N-GNS nanocomposite (a) and equivalent circuit model (b).

4. Conclusion

We have successfully prepared hedgehog-like CuO/N-GNS nanocomposite by a hydrothermal method. After 50 cycles, hedgehog-like CuO/N-GNS nanocomposite exhibited higher discharge special capacity (750.1 $mAhg^{-1}$) than hedgehog-like CuO (456.8 $mAhg^{-1}$) at a current of 100 mA g^{-1}. These excellent

performances can be attributed to the N-GNSs with good electrical conductivity which server as a conducting network for fast electron transfer between the active materials and charge collector, as well as buffer spaces to accommodate the volume expansion of CuO during discharge/charge process. The main reason is may be due to N-GNSs can promote the conductivity of hedgehog-like CuO, enlarge the lithium ions to contact with the electrode and shorten lithium ions route of transmission, buffer the change of volume to keep the structure stability during discharging and charging.

Acknowledgment

This work was supported by the National Natural Science Foundation of China (Grant No. 51572012) and Doctoral Fund of Ministry of Education of China (20120010110001).

References

[1] S.M. Abbas, S. Ali, N. Ahmad, Synthesis of carbon nanotubes anchored with mesoporous Co_3O_4, nanoparticles as anode material for lithium-ion batteries, Electrochim. Acta 26 (2013) 481–488.
[2] L.T. Anh, A.K. Rai, T.V. Thi, Improving the electrochemical performance of anatase titanium dioxide by vanadium doping as an anode material for lithium-ion batteries, J. Power Sources 6 (2013) 891–898.
[3] W. Chen, H. Jiang, Y. Hu, Mesoporous single crystals $Li_4Ti_5O_{12}$ grown on rGO as high-rate anode materials for lithium-ion batteries, Chem. Commun. 64 (2014) 2609–2615.
[4] B. Wang, X.L. Wu, C.Y. Shu, Synthesis of CuO/graphene nanocomposite as a high-performance anode material for lithium-ion batteries, J. Mater. Chem. 47 (2010) 10661–10664.
[5] B. Wang, B. Luo, X. Li, The dimensionality of Sn anodes in Li-ion batteries, Mater. Today 12 (2012) 544–552.
[6] M.A. Velasco-Soto, S.A. Pérez-García, J. Alvarez-Quintana, et al., Selective band gap manipulation of graphene oxide by its reduction with mild reagents, Carbon 93 (2015) 967–973.
[7] P. Steurer, R. Wissert, R. Thomann, Functionalized graphenes and thermoplastic nanocomposites based upon expanded graphite oxide, Macromol. Rapid Comm. 30 (2009) 316–327.
[8] H. Chen, F. Feng, H.U. Zhong-Liang, Preparation of uniform hedgehog-like CuO and hedgehog-like CuO/graphene composite and their application in lithium ion batteries, Trans. Nonferrous Met. Soc. China 10 (2012) 2523–2528.
[9] S. Jung, S. Jeon, K. Yong, Fabrication and characterization of hedgehog-like CuO-ZnO heterostructure nanowire arrays by photochemical deposition, Nanotechnology 1 (2011) 184–190.
[10] S.M. Abbas, S.T. Hussain, S. Ali, One-pot synthesis of a composite of monodispersed CuO nanospheres on carbon nanotubes as anode material for lithium-ion batteries, J. Alloy. Compd. 1 (2013) 221–226.
[11] F. Nouroozi, F. Farzaneh, Synthesis and characterization of brush-like ZnO nanorods using albumen as biotemplate, J. Braz. Chem. Soc. 3 (2011) 484–488.
[12] S.M. Abbas, S.T. Hussain, S. Ali, One-pot synthesis of a composite of monodispersed CuO nanospheres on carbon nanotubes as anode material for lithium-ion batteries, J. Alloy. Compd. 1 (2013) 221–226.
[13] W. Chen, C. Qian, X.Y. Liu, A two-dimensional correlation spectroscopic analysis on the interaction between humic acids and TiO_2 nanopaticles, Environ. Sci. Technol. 19 (2015) 11119–11126.
[14] K.F. Darling, M. Kucera, C.M. Wade, Seasonal distribution of genetic types of planktonic foraminifer morphospecies in the Santa Barbara Channel and its paleoceanographic implications, Paleoceanography 2 (2003) 1–10.
[15] F. Fontani, M.T. Beltran, J. Brand, Search for massive protostellar candidates in the southern hemisphere: I. association with dense gas, Astron. Astrophys. A Eur. J. 1 (2004) 221–234.
[16] J.F. González, A. Ramiro, C.M. Gonzálezgarcía, Pyrolysis of almond shells. Energy applications of fractions, Ind. Eng. Chem. Res. 9 (2005) 3003–3012.
[17] B. Tian, J. Światowska, V. Maurice, et al., Combined surface and electrochemical study of the lithiation/delithiation mechanism of the iron oxide thin-film anode for lithium-ion batteries, J. Phys. Chem. C 42 (2013) 21651–21661.
[18] A. Fernández, F. Martín, J. Morales, et al., Beneficial effects of Mo on the electrochemical properties of tin as an anode material for lithium batteries, Electrochim. Acta 17 (2006) 3391–3398.
[19] W. Si, X. Sun, X. Liu, High areal capacity, micrometer-scale amorphous Si film anode based on nanostructured Cu foil for Li-ion batteries, J. Power Sources 3 (2014) 629–634.
[20] H. Dai, C.K. Thai, M. Sarikaya, Through-mask anodic patterning of copper surfaces and film stability in biological media, Langmuir 8 (2004), 6–3483.
[21] Z. Zhang, H. Chen, X. She, Synthesis of mesoporous copper oxide microspheres with different surface areas and their lithium storage properties, J. Power Sources 11 (2012) 336–344.
[22] J.D.C. Jacob, T.R. Lee, S. Baldelli, In situ vibrational study of the reductive desorption of alkanethiol monolayers on gold by sum frequency generation spectroscopy, J. Phys. Chem. C 50 (2014) 29126–29134.
[23] J. Liu, H. Xia, L. Lu, Anisotropic Co_3O_4 porous nanocapsules toward high-capacity Li-ion batteries, J. Mater. Chem. 20 (2010) 1506–1510.
[24] Y. Liu, W. Wang, H. Huang, The highly enhanced performance of lamellar WS_2 nanosheet electrodes upon intercalation of single-walled carbon nanotubes for supercapacitors and lithium ions batteries, Chem. Commun. 34 (2014), 8–4485.
[25] L. Gan, H. Guo, Z. Wang, A facile synthesis of graphite/silicon/graphene spherical composite anode for lithium-ion batteries, Electrochim. Acta 8 (2013) 117–123.
[26] X. Zhang, D. Luo, G. Li, Self-adjusted oxygen-partial-pressure approach to the improved electrochemical performance of electrode $Li[Li_{0.14}Mn_{0.47-}Ni_{0.25}Co_{0.14}]O_2$ for lithium-ion batteries, J. Mater. Chem. A 1 (2013) 9721–9729.
[27] S. Hwang, S.L. Bang, Y.S. Chi, Faradaic impedance titration and control of electron transfer of 1-(12-mercaptododecyl) imidazole monolayer on a gold electrode, Electrochim. Acta 5 (2008) 2630–2636.